Quantitative Fundus Autofluorescence and Optical Coherence Tomography in *ABCA4* Carriers

Tobias Duncker,[1] Gregory E. Stein,[1] Winston Lee,[1] Stephen H. Tsang,[1,2] Jana Zernant,[1] Srilaxmi Bearelly,[1] Donald C. Hood,[1,3] Vivienne C. Greenstein,[1] François C. Delori,[4] Rando Allikmets,[1,2] and Janet R. Sparrow[1,2]

[1]Department of Ophthalmology, Columbia University, New York, New York, United States
[2]Department of Pathology and Cell Biology, Columbia University, New York, New York, United States
[3]Department of Psychology, Columbia University, New York, New York, United States
[4]Schepens Eye Research Institute and Department of Ophthalmology, Harvard Medical School, Boston, Massachusetts, United States

Correspondence: Janet R. Sparrow, Department of Ophthalmology, Columbia University, 635 West 165th Street, New York, NY 10032, USA; jrs88@cumc.columbia.edu.

Submitted: May 29, 2015
Accepted: September 30, 2015

Citation: Duncker T, Stein GE, Lee W, et al. Quantitative fundus autofluorescence and optical coherence tomography in *ABCA4* carriers. *Invest Ophthalmol Vis Sci*. 2015;56:7274–7285. DOI:10.1167/iovs.15-17371

Purpose. To assess whether carriers of *ABCA4* mutations have increased RPE lipofuscin levels based on quantitative fundus autofluorescence (qAF) and whether spectral-domain optical coherence tomography (SD-OCT) reveals structural abnormalities in this cohort.

Methods. Seventy-five individuals who are heterozygous for *ABCA4* mutations (mean age, 47.3 years; range, 9–82 years) were recruited as family members of affected patients from 46 unrelated families. For comparison, 57 affected family members with biallelic *ABCA4* mutations (mean age, 23.4 years; range, 6–67 years) and two noncarrier siblings were also enrolled. Autofluorescence images (30°, 488-nm excitation) were acquired with a confocal scanning laser ophthalmoscope equipped with an internal fluorescent reference. The gray levels (GLs) of each image were calibrated to the reference, zero GL, magnification, and normative optical media density to yield qAF. Horizontal SD-OCT scans through the fovea were obtained and the thicknesses of the outer retinal layers were measured.

Results. In 60 of 65 carriers of *ABCA4* mutations (age range, 9–60), qAF levels were within normal limits (95% confidence level) observed for healthy noncarrier subjects, while qAF levels of affected family members were significantly increased. Perifoveal fleck-like abnormalities were observed in fundus AF images in four carriers, and corresponding changes were detected in the outer retinal layers in SD-OCT scans. Thicknesses of the outer retinal layers were within the normal range.

Conclusions. With few exceptions, individuals heterozygous for *ABCA4* mutations and between the ages of 9 and 60 years do not present with elevated qAF. In a small number of carriers, perifoveal fleck-like changes were visible.

Keywords: Abca4, heterozygous carrier, lipofuscin, optical coherence tomography, quantitative fundus autofluorescence, recessive Stargardt disease, retinal pigment epithelium, scanning laser ophthalmoscope

The adenosine triphosphate-binding cassette, subfamily A, member 4 (*ABCA4*) gene, which is located on the short arm of chromosome 1, encodes for a membrane-associated protein located in outer segment (OS) disc membranes of rod and cone photoreceptors.[1,2] ABCA4, originally identified as rim protein,[3] participates in the transfer of retinaldehyde from the interior of the OS disc to the cytosol, after photobleaching of rhodopsin. Failure of this process leads to an increased formation of bisretinoid fluorophores due to condensation reactions of retinaldehyde; these fluorophores subsequently accumulate in the retinal pigment epithelium (RPE) as lipofuscin.[4–6] Numerous toxic effects of bisretinoid have been demonstrated in in vitro studies.[7] Additionally, in *Abca4*$^{-/-}$ mice that accumulate bisretinoids such as A2E in abundance, photoreceptor cells degenerate.[8] Although accumulation of RPE lipofuscin, albeit at lower levels, is also part of the normal aging process, it is widely accepted that excessive accumulation of RPE lipofuscin is the damaging agent in recessive Stargardt disease (STGD1).[9,10] The role of lipofuscin accumulation in age-related macular degeneration (AMD), a complex multifactorial disease, remains to be determined.

Homozygous and compound heterozygous *ABCA4* mutations are associated with multiple retinal dystrophy phenotypes including autosomal recessive STGD1, cone-rod dystrophy-3, and retinitis pigmentosa-19.[11–14] Although establishing genotype–phenotype correlations has met with difficulty, given the extraordinary allelic heterogeneity in *ABCA4* with currently more than 800 known disease-associated genetic variants, *ABCA4*-related disease is thought to be inversely correlated with the residual ABCA4 activity. For instance, patients with a severe reduction in *ABCA4* activity manifest early and severe phenotypic changes. Approximately 5% of individuals of European descent carry a disease-associated *ABCA4* allele.[15,16] This high carrier frequency has implications for the extent to which *ABCA4* variants contribute to the burden of retinal disease. Carriers of *ABCA4* mutations may be at an increased risk of developing AMD,[17–20] may reveal subtle visual dysfunc-

Table 1. Heterozygous *ABCA4* Carriers: Summary of Demographic, Clinical, and Genetic Data

Subject	Sex	Age	Race/ Ethnicity	Relationship to Proband	*ABCA4* Mutation	BCVA, logMAR		Eye Segmented	qAF_8	
						OD	OS		OD	OS
S1.3	F	48.3	White	Mother	p.[L541P;A1038V]	0.18	0.00	OD	357	339
S1.4	M	49.2	White	Father	c.768+358C>T	0.00	0.00	OS	322	339
S1.5	M	24.7	White	Half-brother	p.[L541P;A1038V]	0.00	0.00	n/a	264	n/a
S1.6	M	9.7	White	Brother	p.[L541P;A1038V]	0.10	0.10	OS	n/a	141
S2.2	F	44.4	Indian	Mother	c.6729+5_+19del	0.10	0.00	OS	257	291
S2.3	M	56.2	Indian	Father	p.G1961E	0.00	0.00	OD	475	431
S3.4	F	54.1	White	Mother	p.G863A	0.00	0.00	OS	459	451
S3.5	F	82.0	White	Grandmother	p.G863A	0.00	0.00	OD	n/a	n/a
S4.2	F	44.6	White	Mother	p.W855*	0.00	0.00	OD	330	n/a
S4.3	M	40.9	White	Father	p.T1526M	0.00	0.00	OS	283	271
S5.2	F	71.5	White	Sister	p.C698Y	0.00	0.10	OD	n/a	n/a
S5.3	F	67.5	White	Sister	c.2160+1G>C	0.00	0.00	OS	n/a	n/a
S5.4	F	62.9	White	Sister	p.C698Y	0.00	0.00	OD	n/a	n/a
S6.2	M	54.9	Black	Brother	p.T1526M	0.10	0.00	OS	477	423
S7.2	F	48.9	White	Mother	c.5196+1G>A	0.00	0.00	OS	443	415
S8.2	F	59.6	White	Mother	p.K346T	0.00	0.00	OD	546	483
S8.3	M	54.6	White	Father	p.T1117I	0.10	0.10	OD	289	n/a
S9.2	F	51.5	White	Mother	c.5196+1137G>A	0.00	0.00	n/a	302	n/a
S9.3	M	57.8	White	Father	p.C54Y	0.00	0.00	OS	419	375
S10.2	M	24.1	Indian	Brother	p.Q2220*	0.00	0.00	OD	227	227
S11.2	F	40.0	Asian	Mother	c.5923del	0.00	0.18	OD	229	191
S11.3	M	40.1	Asian	Father	p.R408*	0.00	0.00	OD	195	178
S12.2	F	53.2	White	Mother	p.L2027F	0.00	0.00	n/a	355	309
S13.2	F	49.8	White	Mother	p.R1161S	0.00	0.00	OS	367	372
S13.3	M	22.3	White	Brother	p.R1161S	0.00	0.00	OD	202	206
S14.2	F	67.0	White	Mother	p.P1380L	0.00	0.00	OD	n/a	n/a
S14.3	F	24.4	White	Sister	p.P1380L	0.00	0.00	OS	n/a	163
S15.3	F	26.8	White	Sister	c.3050+5G>A	0.00	0.00	n/a	293	281
S16.2	M	53.7	Black	Father	c.4253+5G>T	0.00	0.00	n/a	n/a	204
S17.2	F	60.0	Hispanic	Mother	p.A1038V	0.00	0.00	n/a	247	n/a
S18.2	F	41.8	Indian	Father	c.5917del	0.00	0.00	OD	n/a	194
S18.3	M	48.6	Indian	Mother	c.859-9T>C	0.00	0.00	OD	253	215
S18.4	F	12.9	Indian	Sister	c.5917del	0.00	0.00	OD	84	93
S19.4	F	58.5	White	Mother	p.L2027F	0.00	0.00	OD	205	n/a
S19.5	M	61.6	White	Father	p.G851D	0.10	0.10	OD	n/a	n/a
S20.2	F	41.5	White	Mother	c.5312+1G>A	0.00	0.00	n/a	335	351
S20.3	M	39.0	White	Father	p.R2030*	0.00	0.10	n/a	442	n/a
S21.3	F	53.1	White	Mother	p.G1961E	0.00	0.00	OD	490	488
S22.3	M	46.3	White	Father	p.L2027F	0.00	0.00	OS	386	376
S22.4	F	47.1	White	Mother	p.[L541P;A1038V]	0.00	0.00	OS	342	326
S23.2	F	37.4	White	Sister	p.G1961E	0.00	0.00	OS	220	n/a
S24.2	F	37.5	White	Daughter	c.247_250dup	0.00	0.00	OD	298	288
S25.3	F	49.9	Black	Mother	p.R2107H	0.88	0.10	n/a	n/a	385
S26.3	F	58.2	White	Mother	p.G1961E	0.00	0.00	OD	238	297
S26.4	M	57.2	White	Father	p.[L541P;A1038V]	0.18	1.30	OS	312	279
S26.3	M	17.4	White	Brother	p.[L541P;A1038V]	0.10	0.00	OS	174	143
S27.2	F	46.2	White	Mother	p.P1380L	0.00	0.10	OD	379	320
S27.3	M	47.3	White	Father	p.G1961E	0.00	0.00	OD	413	384
S27.4	F	17.4	White	Sister	p.P1380L	0.00	0.00	OS	184	189
S28.2	F	58.9	White	Mother	p.[A854T;A1038V]	0.00	0.00	OS	n/a	449
S29.2	F	26.8	White	Daughter	p.A848D	0.00	0.00	OD	n/a	246
S30.2	F	63.5	Hispanic	Sister	p.R1300*	0.00	0.00	n/a	n/a	n/a
S31.2	M	49.7	White	Father	p.[Y245*;V767D]	0.00	0.00	OS	366	368
S32.2	F	54.3	Hispanic	Mother	p.[W1408R;R1640W]	0.00	0.00	n/a	n/a	336
S33.2	F	46.5	White	Mother	p.G1961E	0.00	0.00	OD	422	n/a
S33.3	M	48.0	White	Father	p.R2030Q	0.00	0.00	OD	298	n/a
S34.2	M	50.3	White	Brother	p.G1961E	0.00	0.48	n/a	394	368
S35.2	F	55.7	White	Mother	p.G1961E	0.00	0.00	OS	328	362
S35.3	M	57.4	White	Father	c.3050+5G>A	0.00	0.00	OD	n/a	265
S36.2	F	59.4	Hispanic	Mother	p.G1961E	0.00	0.00	OS	380	374
S37.2	F	55.1	White	Mother	p.G1961E	0.00	0.00	n/a	n/a	352
S38.2	F	48.9	White	Mother	p.W821R	0.00	0.00	OD	252	279

Table 1. Continued

Subject	Sex	Age	Race/ Ethnicity	Relationship to Proband	*ABCA4* Mutation	BCVA, logMAR		Eye Segmented	qAF_8	
						OD	OS		OD	OS
S38.3	M	50.9	White	Father	p.C2150Y	0.00	0.00	OS	336	380
S39.3	F	42.5	White	Mother	c.5714+5G>A	0.00	0.00	n/a	462	393
S39.4	F	18.4	White	Sister	c.5714+5G>A	0.00	0.00	n/a	222	212
S40.2	F	50.1	White	Mother	p.R2030Q	0.00	0.00	OD	433	n/a
S40.3	M	48.8	White	Father	p.K1547*	0.00	0.00	OS	n/a	477
S41.2	F	60.3	White	Mother	p.C54Y	0.00	0.00	OS	n/a	n/a
S42.2	F	44.5	White	Mother	p.Q1412*	0.10	0.00	OS	264	291
S42.3	M	44.2	White	Father	p.R1108C	0.30	0.18	OD	264	232
S43.2	F	44.9	White	Mother	p.G1961E	0.00	0.00	OS	404	n/a
S44.3	M	37.1	Asian	Father	c.4248_4250del	0.00	0.00	OD	307	317
S45.2	F	66.3	White	Mother	p.N965Y	0.18	0.40	n/a	n/a	n/a
S45.3	M	68.0	White	Father	p.P1486L	0.00	0.00	n/a	n/a	n/a
S46	M	32.3	White	Spouse†	p.T897I	−0.12	−0.12	OD	194	200

BCVA, best-corrected visual acuity; logMAR, logarithm of the minimum angle of resolution; OD, right eye; OS, left eye; qAF_8, average quantitative autofluorescence of the 8 measurement sites from all available images per eye; n/a, not available.

† Spouse of P36.1 obtained screening for purposes of family planning.

tion in psychophysical and electrophysiological tests,[21] and may demonstrate moderate to severe fundus changes.[17,22]

The increased accumulation of lipofuscin in the RPE of patients with biallelic mutations in *ABCA4* has been documented by histology,[9] by spectrofluorometry,[23] and more recently by quantitative autofluorescence (qAF).[24] It is still unknown, however, whether individuals heterozygous for *ABCA4* mutations also have elevated lipofuscin levels due to reduced *ABCA4* activity. Data from the *Abca4* mouse model support this hypothesis. Thus we and others[25,26] have found that in mice heterozygous for a null mutation in *Abca4*, A2E levels are elevated relative to those in wild-type.

In this study we used qAF to measure the effect of monoallelic *ABCA4* mutations on RPE lipofuscin levels. Essential to the qAF methodology are an internal fluorescent reference installed in the confocal scanning laser ophthalmoscope (cSLO) and a rigorous protocol for image acquisition. Measurement of fundus AF levels is enabled by an internal reference, which is imaged simultaneously with the fundus to account for changes in laser power over time and to adjust for differences in the sensitivity setting of the cSLO.[27] In addition, fundus AF gray levels are corrected for magnification and optic media density. We also analyzed spectral-domain optical coherence tomography (SD-OCT) scans acquired from carriers of *ABCA4* mutations to assess whether structural alterations could be observed.

Methods

Genetic Testing and Subjects

Asymptomatic carriers (subjects, S) of *ABCA4* mutant alleles were recruited prospectively after disease-causing mutations in *ABCA4* were confirmed in their affected family member (probands, P). In one case (S39) the carrier was screened for the purpose of family planning. Screening of clinically diagnosed STGD1 patients involved various versions of the *ABCA4* chip, including early chips (~300 mutations) and more recent versions of the array (>600 variants). When array screening identified only one mutated *ABCA4* allele or no *ABCA4* mutations, next-generation sequencing (NGS) was carried out. In the latter case, the 50 exons and exon–intron boundaries of the *ABCA4* gene were amplified (Illumina TruSeq Custom Amplicon protocol; Illumina, San Diego, CA, USA) and then submitted to NGS on the Illumina MiSeq platform with analysis using the variant discovery software NextGENe (SoftGenetics LLC, State College, PA, USA) and reference genome GRCh37/hg19. Variants were confirmed by Sanger sequencing and analyzed with Alamut software (http://www.interactive-biosoftware.com [in the public domain]). After confirming the mutations in the proband, screening of the identified mutations by direct Sanger sequencing was carried out in the parents and siblings of the proband.

Seventy-five individuals heterozygous for disease-causing *ABCA4* mutations from 46 unrelated families were recruited between December 2011 and December 2014. The mean age of the carrier cohort was 47.3 years; range was 9 to 82 years, and 46 of the subjects were females. Table 1 summarizes demographic and genetic information of the carriers and their familial relationship to the probands (54 parents, 17 siblings, 2 progeny, 1 grandparent, 1 spouse sequenced for family planning). Sixty-five of these carriers were aged 60 and below and thus could be included in the qAF analysis. The remaining 10 carriers were included in the study as part of our examination for fundus changes.

For comparison, we also included 57 affected family members with biallelic *ABCA4* mutations in the study. The mean age of the *ABCA4*-patient cohort was 23.4 years; range was 7 to 67 years, and 35 of the patients were females. Demographic and genetic information of the affected family members with biallelic *ABCA4* mutations is presented in Table 2. For an intrafamily comparison of qAF levels, we also included two noncarrier siblings in the study (S39.5, S27.5).

All subjects were examined by a retinal specialist. Snellen visual acuity, converted to logMAR visual acuity, was obtained using the most recent refractive correction. All procedures adhered to the tenets of the Declaration of Helsinki, and written informed consent was obtained from all subjects after a full explanation of the procedures was provided. The protocol was approved by the Institutional Review Board of Columbia University.

Study subjects included in the qAF analysis (see below) were compared to our database of 374 healthy eyes of 277 subjects (age 5–60 years) that was reported previously.[28] This group of subjects included the following ethnicities and ages (mean age, age range): 87 whites (31.8, 6–58), 79 Hispanics (30.1, 5–60), 47 blacks (36.6, 9–56), 43 Asians (36.5, 22–59), 6

Table 2. Biallelic *ABCA4* Patients: Summary of Demographic, Clinical, and Genetic Data

Patient	Sex	Age	Race/ Ethnicity	*ABCA4* Mutation		BCVA, logMAR		qAF_8	
				Allele 1	Allele 2	OD	OS	OD	OS
P 1.1§	M	11.4	White	p.[L541P;A1038V]	c.768+358C>T	0.54	0.60	639	627
P 1.2§	M	7.0	White	p.[L541P;A1038V]	c.768+358C>T	0.30	0.18	n/a	413
P 2.1†	M	17.9	Indian	p.G1961E	c.6729+5_+19del	0.70	0.88	340	363
P 3.1§	F	25.1	White	p.G863A	c.5898+1G>A	0.80	0.80	710	675
P 3.2†	F	18.9	White	p.G863A	c.5898+1G>A	0.00	0.00	465	431
P 3.3	F	24.4	White	p.G863A	c.5898+1G>A	0.18	0.00	507	467
P 4.1	M	9.0	White	p.W855*	p.T1526M	1.00	1.00	538	n/a
P 5.1	F	67.0	White	p.C54Y	c.2160+1G>C	CF	HM	n/a	n/a
P 6.1	M	46.0	Black	p.T1526M		0.30	0.80	n/a	n/a
P 7.1	F	25.3	White	c.5196+1G>A	p.S2235P	1.00	1.30	420	317
P 8.1	M	17.0	White	p.K346T	p.T1117I	1.30	0.70	871	828
P 9.1	M	21.5	White	p.C54Y	c.5196+1137G>A	0.18	0.18	609	608
P 10.1	M	31.0	Indian	c.[66G>A;859-9T>C]	p.Q2220*	CF	1.30	n/a	n/a
P 11.1	M	15.0	Asian	p.R408*	c.5935del	1.10	1.30	n/a	n/a
P 12.1§	M	15.1	White	p.L2027F	p.R2077W	0.80	0.80	728	697
P 13.1§	F	23.8	White	p.R1161S		0.60	0.40	571	647
P 14.1§	F	27.3	White	p.P1380L	p.P1380L	1.30	1.00	n/a	577
P 15.1	M	17.0	White	p.G1961E	c.3050+5G>A	0.88	0.88	n/a	n/a
P 15.2	F	22.0	White	p.G1961E	c.3050+5G>A	0.88	0.88	n/a	n/a
P 16.1	F	19.1	Black	p.V989A	c.4253+5G>T	0.30	0.40	97	n/a
P 17.1	F	21.8	Hispanic	p.A1038V	p.G1441D	0.70	0.88	551	528
P 18.1	M	22.0	Indian	c.859-9T>C	c.5917del	0.88	0.88	527	n/a
P 19.1§	F	27.2	White	p.G851D	p.L2027F	0.88	0.88	448	459
P 19.2§	F	29.2	White	p.G851D	p.L2027F	1.30	1.18	538	569
P 19.3	F	34.2	White	p.G851D	p.L2027F	1.00	1.30	442	n/a
P 20.1	F	9.5	White	c.5312+1G>A	p.R2030*	0.88	0.70	998	929
P 21.1†	F	24.6	White	p.N96D	p.G1961E	0.30	0.18	513	549
P 21.2†	F	20.9	White	p.N96D	p.G1961E	0.30	0.40	397	355
P 22.1	M	8.0	White	p.[L541P;A1038V]	p.L2027F			n/a	n/a
P 22.2	M	13.9	White	p.[L541P;A1038V]	p.L2027F	0.30	0.40	591	608
P 23.1†	F	26.0	White	p.G1961E	c.5196+1056A>G	0.40	0.70	379	344
P 24.1	F	52.0	White	c.247_250dup		0.80	0.00	n/a	n/a
P 25.1	F	26.0	Black	p.E526A	p.R2107H	0.48	0.00	507	536
P 25.2	F	25.9	Black	p.E526A	p.R2107H	0.18	0.00	461	468
P 26.1§	F	25.6	White	p.[L541P;A1038V]	p.G1961E	0.60	0.60	n/a	398
P 26.2	F	19.7	White	p.[L541P;A1038V]	p.G1961E	0.60	0.54	320	307
P 27.1§	F	18.8	White	p.P1380L	p.G1961E	0.60	0.70	368	n/a
P 28.1§	F	22.9	White	p.[A854T;A1038V]	p.C2150Y	0.88	0.80	n/a	512
P 29.1§	F	52.2	White	p.A848D	p.A1038V	1.00	1.00	n/a	459
P 30.1	F	40.3	Hispanic	p.F938S	p.R1300*	0.40	1.18	524	451
P 31.1	M	6.0	White	p.[Y245*;V767D]		1.30	1.30	n/a	n/a
P 32.1	F	32.0	Hispanic	p.H1118Y	p.[W1408R;R1640W]	1.00	1.00	n/a	n/a
P 33.1§	M	23.0	White	p.R2030Q	p.G1961E	1.00	1.00	334	347
P 34.1	M	46.9	White	p.C1490Y	p.G1961E	0.40	0.30	376	384
P 35.1‡	M	24.8	White	c.3050+5G>A	p.G1961E	0.00	0.00	381	451
P 36.1‡	F	29.3	Hispanic	p.L541P	p.G1961E	0.40	0.40	479	487
P 37.1†	F	24.7	White	p.G1961E	p.C2150R	0.88	0.88	405	396
P 38.1§	M	11.7	White	p.W821R	p.C2150Y	0.40	0.40	306	n/a
P 39.1	F	12.8	White	p.P1380L	c.5714+5G>A	0.60	0.40	558	573
P 39.2	M	14.1	White	p.P1380L	c.5714+5G>A	0.88	0.88	395	462
P 40.1†	F	16.2	White	p.K1547*	p.R2030Q	0.70	0.40	481	513
P 41.1	F	19.0	White	p.C54Y		0.88	0.88	n/a	n/a
P 42.1†	F	13.0	White	p.R1108C	p.Q1412*	1.30	1.00	511	528
P 43.1†	M	17.4	White	p.A1773V	p.G1961E	0.88	0.88	340	366
P 44.1	M	14.0	Asian	p.R408*	c.4248_4250del	1.30	1.30	n/a	n/a
P 44.2	F	7.0	Asian	p.R408*	c.4248_4250del	1.30	1.30	n/a	n/a
P 45.1	F	42.4	White	p.N965Y	p.P1486L	0.10	0.40	n/a	n/a

BCVA, best-corrected visual acuity; logMAR, logarithm of the minimum angle of resolution; OD, right eye; OS, left eye; qAF_8, average quantitative autofluorescence of the 8 measurement sites from all available images per eye; n/a, not available.

† Previously published in Duncker et al.[45]

‡ Previously published in Duncker et al.[46]

§ Previously published in Burke et al.[24]

Investigative Ophthalmology & Visual Science

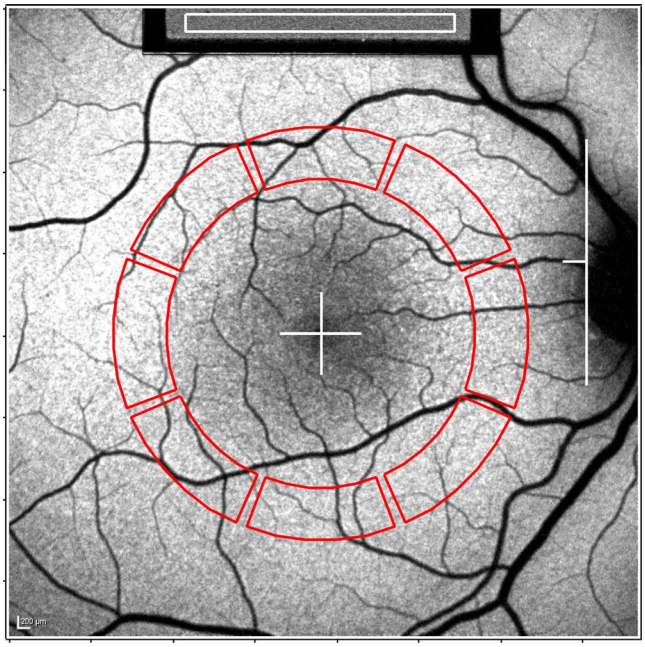

Figure 1. Quantitative fundus autofluorescence image analysis. S22.3. Mean gray levels (GLs) are recorded from the internal reference (*white rectangle*, *top of image*) and from 8 circularly arranged segments (*red*). The segments are scaled to the distance between the temporal edge of the optic disc (*white vertical line*) and the center of the fovea (*white cross*). After accounting for the presence of large vessels, qAF values of the 8 segments are averaged to determine qAF_8.

Indians (32.1, 25–39), and 15 others (27.5, 10–57). Carriers included in the quantitative analysis of the SD-OCT scans (see below) were compared to 46 age-similar control subjects (mean age ± standard deviation [SD], 45.3 ± 15.8 years; range, 11–84 years; 24 females). All but six (ages: 62–84 years) of these controls were subjects from our previously published normative qAF database.[28]

Imaging

Short-wavelength (SW) fundus AF images were acquired with a confocal scanning laser ophthalmoscope (Spectralis HRA-OCT; Heidelberg Engineering, Heidelberg, Germany) modified by the insertion of an internal fluorescent reference to account for variable laser power and detector gain.[27] Excitation was 488 nm, and the barrier filter in the device transmitted light from 500 to 680 nm. All AF images were recorded for a 30° × 30° field (768 × 768 pixels) in the high-speed mode (8.9 frames/s) as a video consisting of either 9 or 12 frames. Before image acquisition, pupils were dilated to at least 7 mm with topical 1% tropicamide and 2.5% phenylephrine, and room lights were dimmed. The camera was aligned in all three dimensions so that the AF beam was located in the center of the pupil and the fundus image was evenly illuminated. The focus was fine-tuned to the point of maximum signal intensity across the fundus. The detector sensitivity was adjusted to avoid nonlinear effects. While these adjustments took place, the fundus was exposed to the AF light for at least 20 seconds to reduce AF attenuation by rod photopigment to <2%.[27] Two or more AF images were recorded, followed by a second imaging session for reproducibility. All videos were reviewed, and those frames without localized or generalized decreased AF signal were aligned, averaged, and saved in "nonnormalized" mode (two images per session).

In addition, a horizontal 9-mm SD-OCT image through the fovea, registered to a simultaneously acquired AF or near-infrared reflectance (NIR-R) image, was recorded in high-resolution mode as an average of 50 to 100 individual images for each eye. Color fundus photography was performed using a FF450+IR fundus camera (Carl Zeiss Meditec, Jena, Germany).

AF Image Analysis

Autofluorescence images were analyzed under the control of an experienced operator (TD, WL) with dedicated image analysis software written in IGOR (WaveMetrics, Lake Oswego, OR, USA).[27] The software recorded the mean GLs of the internal reference and from eight circularly arranged segments positioned at an eccentricity of approximately 7° to 9° (Fig. 1). Segments were scaled to the distance between the fovea and the temporal edge of the optic disc. An algorithm of the software accounted for the presence of vessels in the sampling area.[27] The gray levels (GLs) from the eight circularly arranged segments in each image were calibrated to the reference, zero GL, magnification, and normative optical media density[29] to yield qAF_8. Gray levels were also adjusted to a reference calibration factor calculated using a master fluorescent reference.[27]

SD-OCT Segmentation

Horizontal SD-OCT line scans through the fovea from one eye of the first 58 consecutively recruited carriers of *ABCA4*

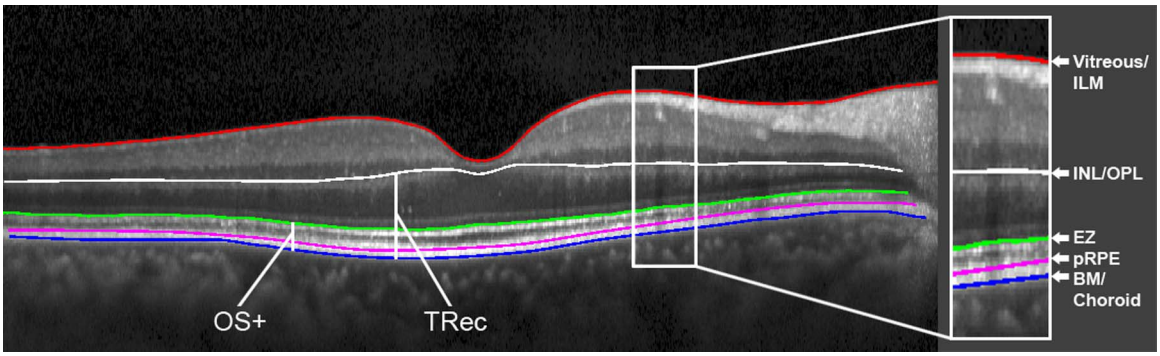

Figure 2. Retinal layer segmentation of SD-OCT scans. Image of horizontal SD-OCT scan from a healthy control subject. Segmented boundaries are indicated as colored lines: *red*, the border between vitreous and inner limiting membrane (ILM); *white*, the border between inner nuclear layer (INL) and outer plexiform layer (OPL); *green*, proximal border of the ellipsoid zone (EZ); *pink*, the proximal border of the retinal pigment epithelium (RPE); and *blue*, the border between Bruch's membrane (BM) and choroid. Two layers were derived from these boundaries: OS+, distance between EZ and BM/choroid; TRec, distance between INL/OPL and BM/choroid.

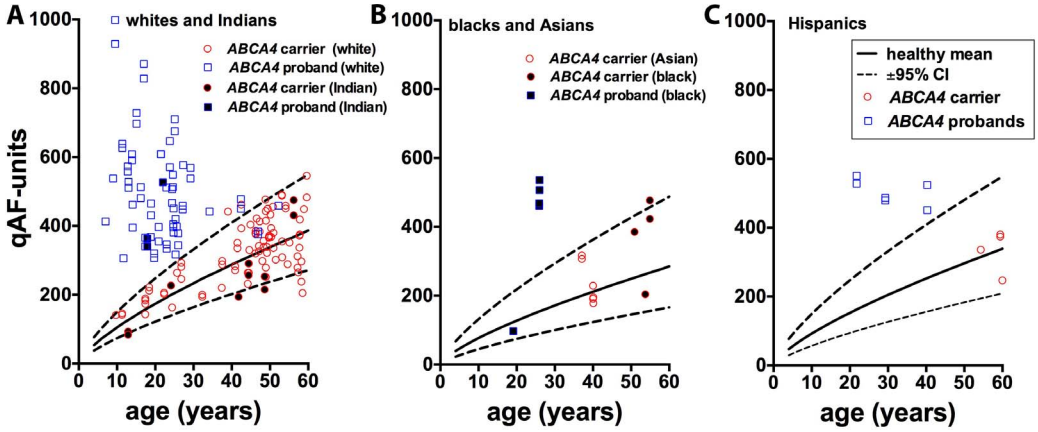

Figure 3. Quantitative fundus autofluorescence intensities plotted as a function of age. Values are the mean of the 8 segments (qAF_8) shown in Figure 1 and measured in carriers of *ABCA4* mutations (*red circles*), *ABCA4*-affected patients (*blue squares*), and subjects with healthy eyes (mean, *solid line*; upper and lower limits [95% confidence level], *dotted lines*) of (**A**) whites (*unfilled symbols*) and Indians (*filled symbols*), (**B**) blacks (*filled symbols*) and Asians (*unfilled symbols*), and (**C**) Hispanics. The values for Indian carriers and probands are plotted with white subjects because the upper 95% CI of whites and Indians is similar.[28] Values for both eyes or one eye (23 carriers and 11 affected patients) are plotted.

mutations (see Table 1) were segmented in Matlab (MathWorks, Natick, MA, USA) by one of the authors (GES), using a manually corrected automated program. The segmentation technique has been described previously.[30,31] When SD-OCT scans from both eyes were available, one eye was randomly chosen for analysis. Five borders, as indicated in Figure 2, were segmented: (1) the border between the vitreous and inner limiting membrane (ILM); (2) the border between the inner nuclear layer (INL) and the outer plexiform layer (OPL); (3) the proximal border of the band corresponding to the ellipsoid zone (EZ); (4) the proximal border of the retinal pigment epithelium (pRPE); and (5) the border between Bruch's membrane (BM) and the choroid. The thicknesses of two layers, the OS plus layer (OS+, from the BM/choroid border to the proximal border of the EZ band) and the total receptor layer (TRec, from the BM/choroid border to the OPL/INL border), were determined (Fig. 2).

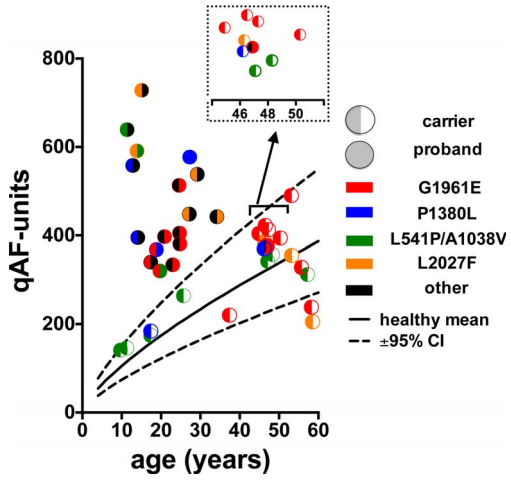

Figure 4. Quantitative autofluorescence intensities associated with 4 common *ABCA4* mutations: p.G1961E, p.P1380L, p.[L541P; A1038V], p.L2027F. Values are plotted for carriers and probands (male and female) as indicated by *colors* and *symbols*. Other *ABCA4* mutations carried by the probands are represented in *black*. Mean (*solid black line*) ± 95% confidence intervals (*dashed lines*) for individuals with healthy eyes are shown. Values are for OD, except in one case where only OS was available. The values (4 carriers and one proband) in the cluster between ages 44 and 52 are replotted in the *inset* above using expanded scales on both axes (*x*, *y*).

Statistical Analyses

Analyses were performed using Prism 5 (GraphPad Software, La Jolla, CA, USA) and the statistical tests as indicated. We used the Bland-Altman method[32] to test the between-session repeatability of qAF measurements and the agreement of qAF measurements between eyes in the carrier population and the *ABCA4*-affected population.

Results

Heterozygous *ABCA4* mutations were detected in 75 subjects from 46 unrelated families. All mutations were known to be disease causing. The following *ABCA4* mutations were frequently present in our cohort: p.G1961E in 11 carriers, p.[L541P; A1038V] in six carriers, p.P1380L in four carriers, and p.L2027F in three carriers. In the group of 57 affected family members, two disease-causing *ABCA4* variants were found in 52 patients (91%) while one disease-causing *ABCA4* variant was detected in the other five patients (Table 2).

Quantitative Fundus Autofluorescence

Since age-related changes in ocular media are more pronounced after age 60, and because our normative database was also limited to that age range,[28] images from subjects and patients above age 60 were not utilized for qAF. Determination of qAF_8 levels was performed on 107 eyes of 65 carriers of *ABCA4* mutations (mean age, 44.3 years; range, 9–60 years). For comparison, we also analyzed the qAF images of 77 eyes of 44 affected family members with biallelic *ABCA4* mutations (mean age, 22.7 years; range, 7–52 years); data from 25 of the patients were published previously (Table 2). All subjects and patients had clear media except for some floaters. The qAF data of the carriers of *ABCA4* mutations presented in this study were based on AF images of 107 eyes, with 82 of these eyes having a second AF imaging session. The qAF data of the 19 not previously reported affected family members with biallelic *ABCA4* mutations presented in this study were based on AF

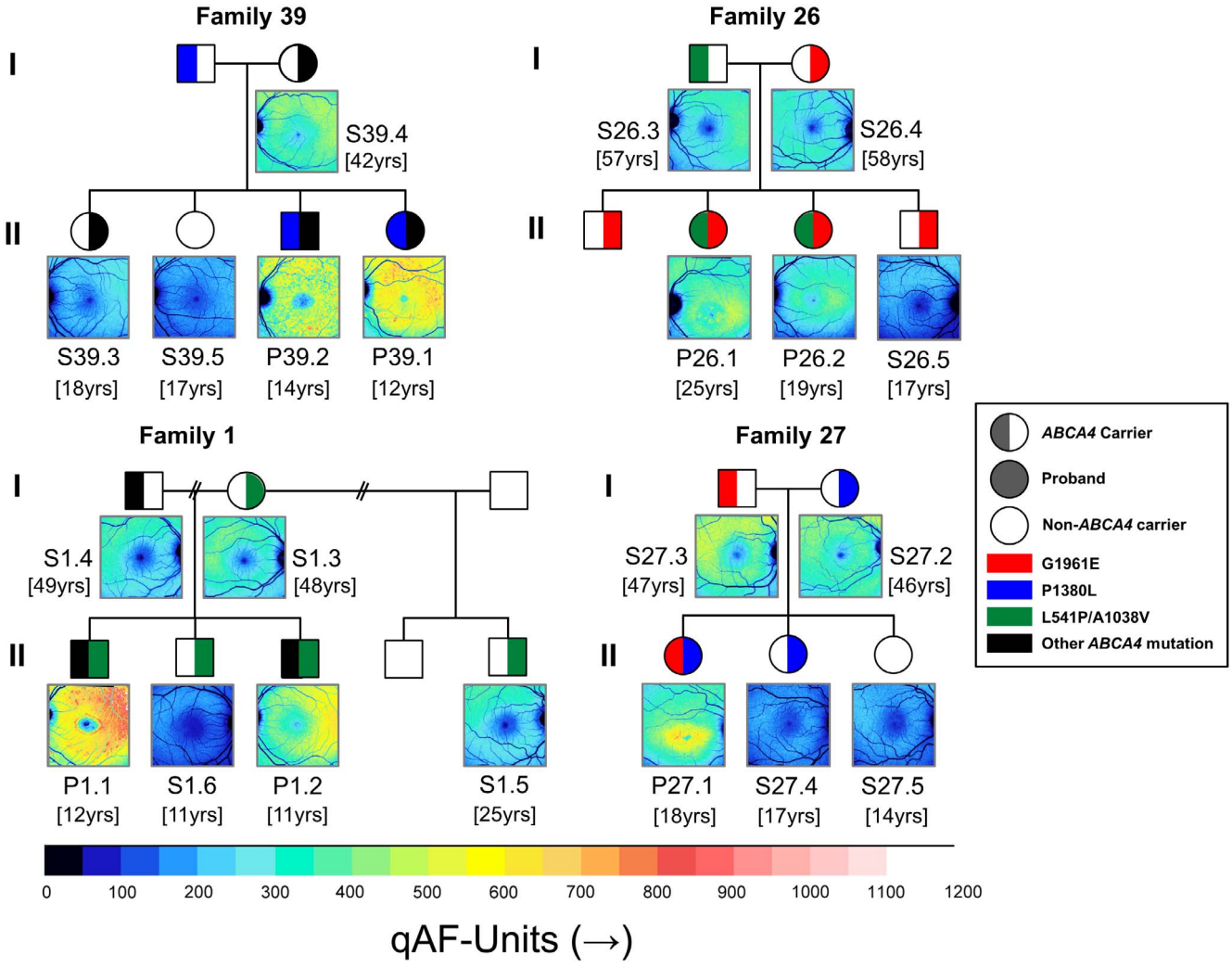

Figure 5. Color-coded maps of quantitative fundus autofluorescence and inheritance patterns of families carrying *ABCA4* mutations p.P1380L (family 39) p.G1961E; p.[L541P, A1038V] (family 26), p.[L541P; A1038V] (family 1), and p.G1961E; p.P1380L (family 27). qAF maps are shown for probands, carriers of *ABCA4* mutations, and non-*ABCA4* carriers; *color-code scale* is shown below. Male, *square*; female, *circle*. Two generations (I, II) are shown for each family. S, subject; P, patient.

images of 34 eyes, with 26 of these eyes having a second AF imaging session.

In 102 of 107 eyes of heterozygous subjects (95%), qAF_8 was within normal limits for age and race/ethnicity (95% confidence level; calculated as 2× SD of the residuals of the mixed effects linear regression analysis, with residuals being the deviations of the observed data points from the predicted values that fit the line) (Fig. 3). Three eyes were above the upper limits (S2.3, OD; S20.3, OD; S38.3, OD), and 2 eyes were below the lower limits (S19.4, OD; S26.3, OD) for healthy subjects. As expected, qAF_8 of the subjects heterozygous for *ABCA4* mutations increased with age. Of the patients affected with *ABCA4*-associated disease, 74 of 77 eyes had qAF_8 levels above the normal limits (95% confidence) for age. In agreement with a previous study,[24] the highest qAF_8 levels were found for younger *ABCA4*-affected patients, while the fold difference relative to normal AF levels was less pronounced for older *ABCA4*-affected patients.

We previously demonstrated that STGD1 patients carrying the p.G1961E mutation on one allele have relatively lower qAF_8 levels compared to patients with p.[L541P; A1038V], p.P1380L, and p.L2027F mutations (and no p.G1961E mutation on the other allele).[24] To determine whether similar differences in the segregation of qAF_8 levels could also be observed for *ABCA4* mutations in carriers and whether specific *ABCA4* mutations may be associated with higher qAF_8 levels, we plotted qAF values for carriers and affected patients who carried one of the four most common mutations (p.G1961E, p.[L541P;A1038V], p.P1380L, and p.L2027F) (Fig. 4). The qAF_8 levels of the carriers appeared to be relatively evenly distributed regardless of the *ABCA4* mutation. Among the carriers, there was no trend for a mutation to be associated with relatively higher or lower qAF_8 levels.

In Figure 5, the pedigrees of families 39, 26, 1, and 27 are shown together with the qAF color maps of all corresponding family members included in the study. While age-similar noncarrier and carriers have comparable qAF levels and a normal spatial distribution of the AF signal, the increased qAF levels of affected family members with biallelic *ABCA4* mutations are immediately discernable from the qAF color maps.

For *ABCA4* carriers, the Bland-Altman coefficient of agreement for qAF_8 of right and left eyes (42 subjects) was ±18.7%, and the between-session Bland-Altman coefficient of repeatability was ±10.3% (n = 82). The coefficient of

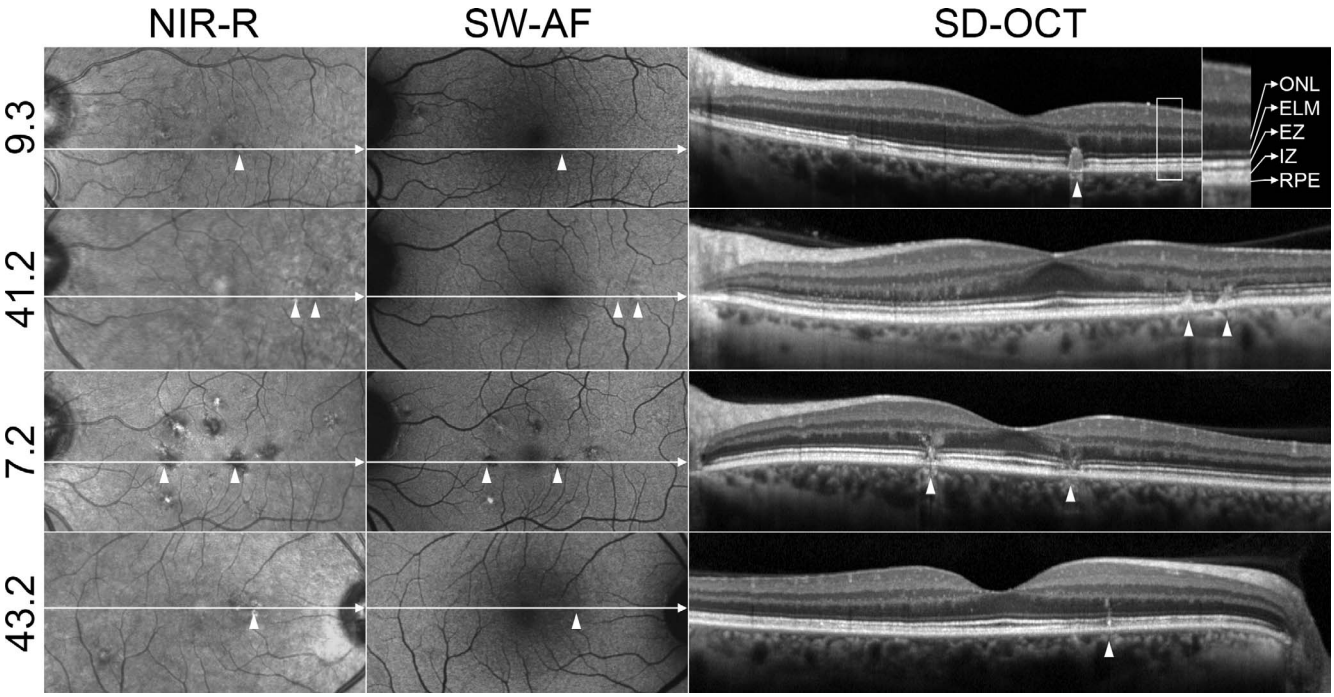

Figure 6. Fundus changes in a subgroup of heterozygous carriers of *ABCA4* mutations. Near-infrared reflectance (NIR-R), short-wavelength fundus autofluorescence (SW-AF), and SD-OCT images of subjects (S) S9.3, S41.2, S7.2, S43.2. The NIR-R and SW-AF images were registered. The axis and horizontal extent of the SD-OCT scan are indicated in the corresponding fundus images. Outer nuclear layer (ONL), external limiting membrane (ELM), photoreceptor ellipsoid zone (EZ), interdigitation zone (IZ), and retinal pigment epithelium/Bruch's membrane (RPE). The nomenclature used for the identification of reflectivity bands in SD-OCT was previously published (Staurenghi et al.).[44] In all 4 subjects, perifoveal fleck-like changes are visible in SD-OCT images; these changes correspond to hyperreflective foci on NIR-R and have an increased AF signal.

agreement for qAF_8 between the right and left eye in affected family members with biallelic *ABCA4* mutations that were not previously reported[24] ($n = 14$) was ±20.5%, and the between-session coefficient of repeatability was ±7.3% ($n = 26$).

Qualitative Analysis of Fundus Images

Fundus images of the recruited carriers of *ABCA4* mutations were also assessed qualitatively. For most subjects, color fundus photography, conventional fundus AF imaging, and SD-OCT were qualitatively unremarkable. However, as shown in Figure 6, four carriers (S9.3, S7.2, S41.2, and S43.2) exhibited fleck-like changes in the perifoveal region. These changes were also visible in color fundus photographs (not shown) and are similar to the flecks seen in STGD1 disease.[33] The foci of increased AF signal corresponded to hyperreflective deposits traversing photoreceptor-attributable bands in SD-OCT images. A fleck that had faded to darkness on AF (temporal fleck, S7.2) presented with hyporeflectivity at the fleck position on OCT.

SD-OCT Thickness Measurements

The first 58 consecutively recruited heterozygous subjects (58 eyes of 58 carriers) were included (mean age, 47.1 years; range, 11–82 years) in the thickness measurements of the OS+ and TRec layers (Table 1). In Figures 7 and 8, the individual SD-OCT thickness profiles of these carriers of *ABCA4* mutations are shown in gray together with the 95% confidence intervals (CI) for controls (mean ± 1.96× standard error of mean [SEM]; [1.96× SD/$\sqrt{}$(n-1)] (bold solid and dashed black lines). In Figure 7, the thickness profiles of S43.2, S7.2, S9.3, and S41.2 are indicated. These subjects exhibited qualitative fundus abnormalities that were visible in SW-AF and SD-OCT (Fig. 6). In Figure 8, the segmentation profiles of carriers expressing the most common mutations, p.G1961E, p.[L541P; A1038V], p.P1380L, and p.L2027F, are indicated in color. While some of the thickness values of the carriers fell above or below the CI of controls, there was no clear trend toward thinning or thickening of the segmented retinal layers throughout the cohort. Interestingly, the variation in the thicknesses measured was greater for OS+ than for TRec profiles.

Discussion

Homozygous and compound heterozygous mutations in the *ABCA4* gene are associated with macular dystrophies that include STGD1 and cone-rod dystrophy.[12,13,18] The inheritance pattern of *ABCA4*-associated disease is exclusively autosomal recessive, and the age of onset of disease is variable. Elevated RPE lipofuscin[9,23] that can be measured as increased qAF[24] is typical of disease linked to *ABCA4* mutations. In our recent study of qAF in STGD1 patients,[24] limited genotype–phenotype correlations were possible. Nevertheless, we concluded that based on qAF values (measured at an eccentricity of 7°–9°), the mutations p.L2027F and p.P1380L and the complex allele p.[L541P; A1038V] conferred a faster rate of lipofuscin accumulation, whereas accumulation in the presence of the p.G1961E and p.G851D mutations was slower. Here we report that carriers of mutations in *ABCA4*, recruited as family members of affected patients, do not exhibit elevated qAF intensities when compared to controls. In a carrier of a mutant allele, half of the protein is defective. Alternatively, there could be posttranscriptional mechanisms that adjust ABCA4 protein to required levels irrespective of whether one or two functional copies of the gene are present.[34]

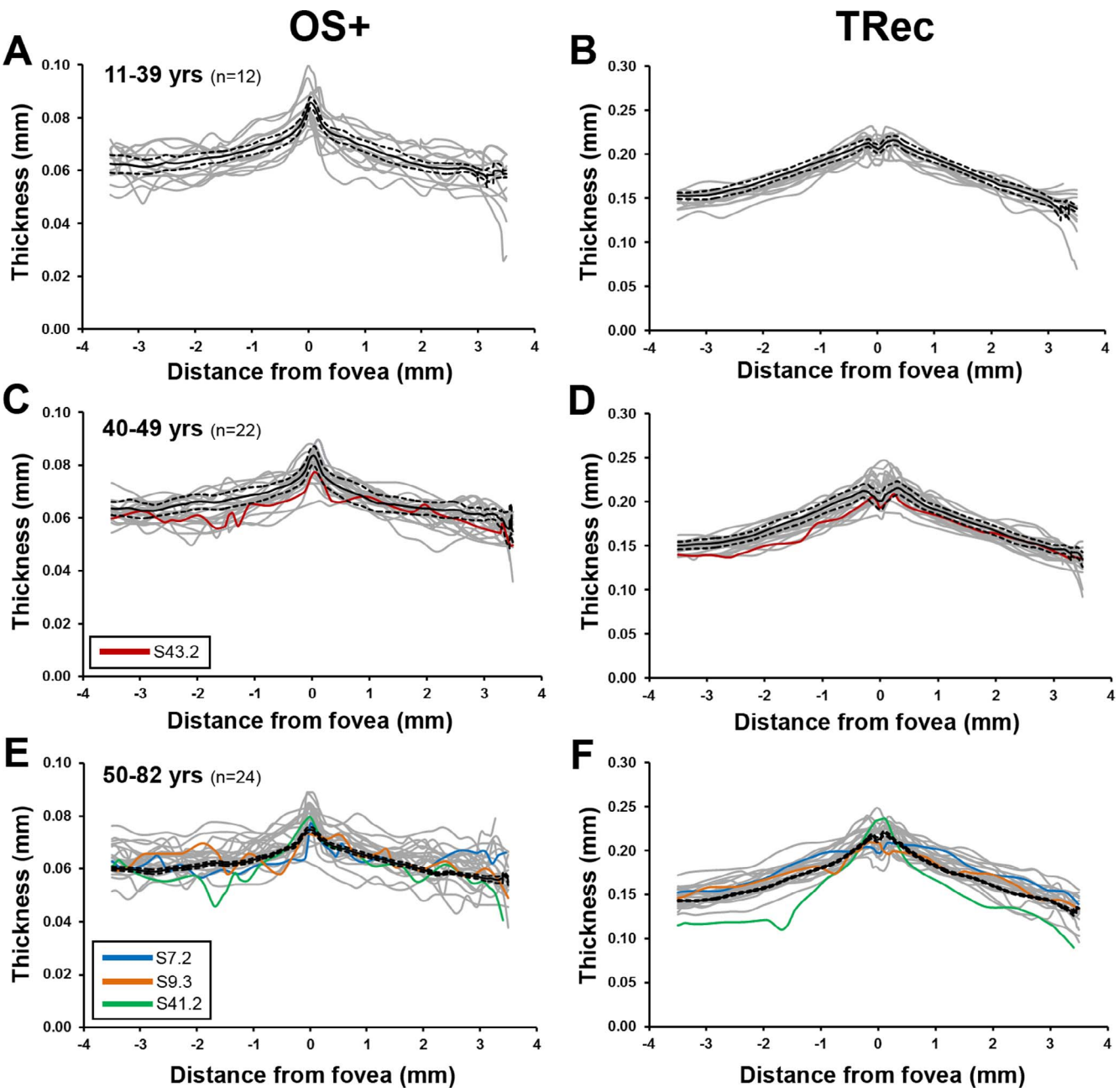

FIGURE 7. Thickness profiles acquired by segmentation of spectral-domain optical coherence tomography (SD-OCT) images of carriers of *ABCA4* mutations. Profiles are shown in *color* for carriers S43.2, S7.2, S9.3, and S41.2; these carriers presented with qualitative fundus changes in SW-AF and SD-OCT as shown in Figure 6. Thickness profiles of individual carriers are shown as gray lines. Thickness profiles of controls are presented as mean (*black solid line*) ± 95% confidence intervals (mean ± 1.96× standard error of mean [SEM]; [1.96× SD/$\sqrt{}$(*n*-1)]; *black dashed lines*). Thicknesses of OS+ layer (from EZ to border between Bruch's membrane and choroid) (**A**, **C**, **E**) and TRec (from border between inner nuclear layer and outer plexiform layer to border between Bruch's membrane and choroid) (**B**, **D**, **F**) are presented as a function of distance from the fovea. Right eyes are presented. Subjects are grouped by ages, and numbers of carriers in each group (*n*) are indicated.

In the *Abca4*$^{-/-}$ mouse, fundus autofluorescence intensities, measured as qAF[26] or corrected gray levels,[35] were found to be 2- to 2.6-fold greater than in wild-type mice, and A2E levels, measured chromatographically, were 4-fold higher.[26] In the heterozygous mice, qAF intensities were increased by approximately 15% while A2E levels were amplified 2-fold. In another study,[25] A2E accumulation was determined to be several-fold higher in *Abca4*$^{\pm}$ than in wild-type mice. We also found that ONL thinning, a measure of photoreceptor cell demise, was a feature of both *Abca4*$^{-/-}$and *Abca4*$^{\pm}$ mice, but the thinning was less pronounced in the latter. With absence of one copy of a gene, as in the *Abca4*$^{\pm}$ heterozygous mouse, the amount of expressed protein is expected to be 50% of that in the wild-type. We do not have corresponding information in human *ABCA4*-associated disease. Several years ago a case–control study of unrelated subjects with AMD identified heterozygous *ABCA4* mutations in a subgroup of AMD cases; six of these patients harbored the p.G1961E mutation.[18] A follow-up study detected the p.G1961E variant statistically significantly more frequently in AMD cases than in matched controls.[36] The p.G1961E mutation is exceptional in that STGD1 patients homozygous for the mutation or compound

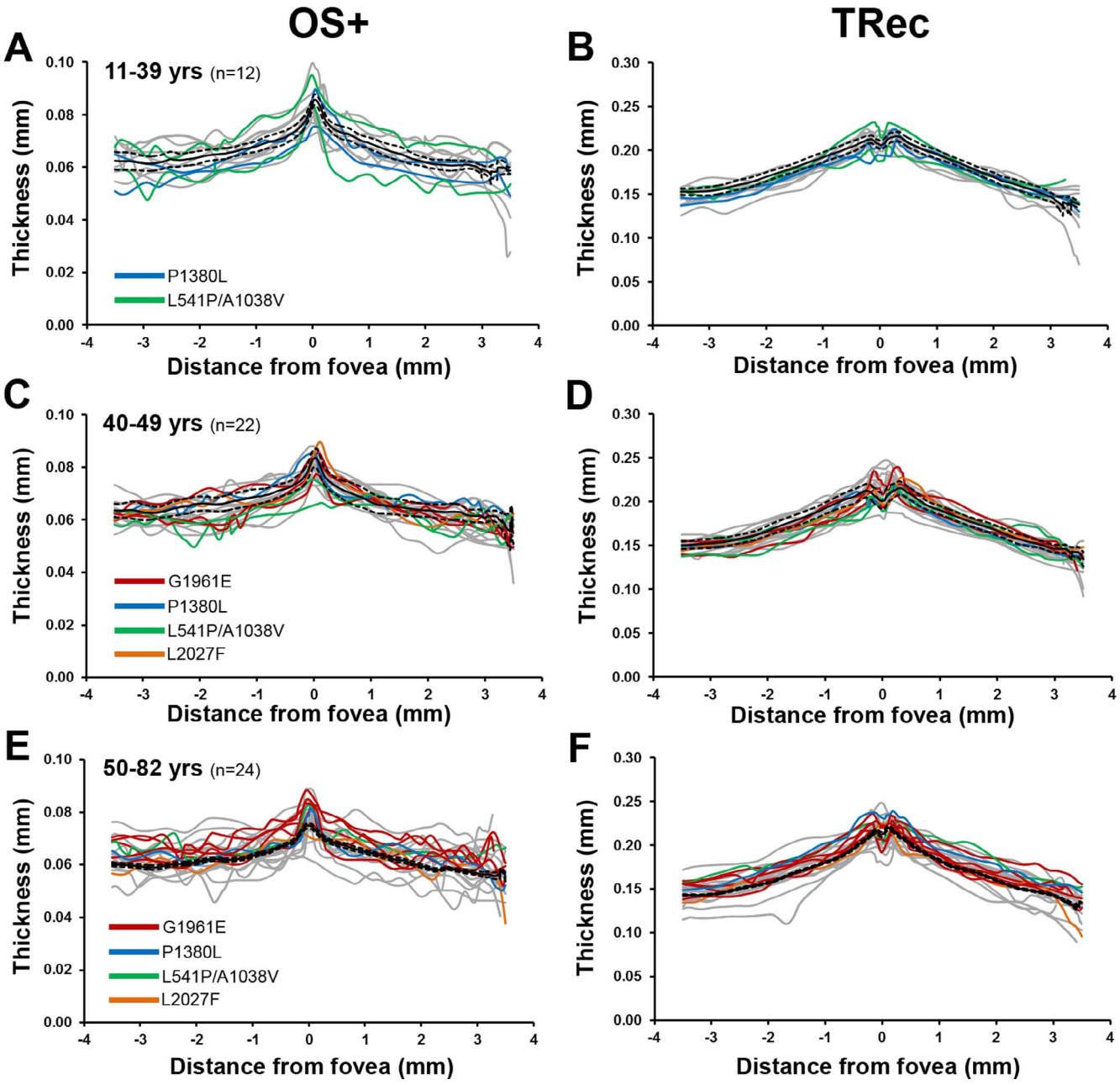

Figure 8. Thickness profiles acquired by segmentation of spectral-domain optical coherence tomography (SD-OCT) images of carriers of *ABCA4* mutations p.G1961E, p.L541P/A1038V, p.P1380L, and p.L2027F. Thicknesses of OS+ layer (from EZ to border between Bruch's membrane and choroid) (**A**, **C**, **E**) and TRec (from border between inner nuclear layer and outer plexiform layer to border between Bruch's membrane and choroid) (**B**, **D**, **F**) are presented as a function of distance from the fovea. Right eyes are presented. Thickness profiles of individual carriers are shown as *gray lines*. Thickness profiles of controls are presented as mean (*black solid line*) ± 95% confidence intervals (mean ± 1.96× standard error of mean [SEM]; [1.96× SD/$\sqrt{}$(*n*-1)]; *black dashed lines*). Subjects are grouped by ages, and numbers of carriers in each group (*n*) are indicated.

heterozygous for p.G1961E and another disease-associated allele exhibit qAF levels (measured 7°–9° from fovea) that are either within the normal range or modestly higher (Fig. 4).[24] These observations with respect to G1961E are consistent with an earlier study wherein most patients with this mutation did not present with a dark choroid during fundus angiography.[37] The dark choroid is thought to be conferred by high lipofuscin levels. Thus since STGD1 patients expressing the G1961E mutation have relatively normal qAF intensities, the finding that carriers of a G1961E mutation also do not exhibit elevated qAF is not informative with respect to the burden of disease.

An association between AMD and heterozygosity for *ABCA4* mutations has not been replicated in all studies,[38,39] yet an analysis of 23 families revealed that carriers of *ABCA4* disease-causing mutations, that is, relatives of STGD1 probands, were significantly more likely than by chance to be affected by AMD.[40] Additionally a subgroup of patients diagnosed with AMD are reported to have geographic atrophy and a SW-AF phenotype that overlaps with STGD1 (fine granular pattern with peripheral punctate spots, GPS[+]). Fritsche et al.[17] demonstrated that patients with the GPS[+] phenotype were often heterozygous for *ABCA4* mutations. This group of patients did not possess the second *ABCA4* mutant allele

required for STGD1; therefore they did not represent late-onset STGD1, which is sometimes phenotypically confused with AMD. The GPS[+] phenotype was most strongly associated with the p.A1038V*ABCA4* allele (5/20 patients). In our cohort, none of the carriers presented with geographic atrophy and the GPS[+] phenotype. Nevertheless, our carrier subjects were significantly younger (range, 11–82 years; mean, 47.3 ± 14.2 years) than the GPS[+] phenotype cohort reported by Fritsche et al. (range, 50–84 years; mean, 63.6 ± 10.4 years).[17] Importantly, Fritsche et al.[17] also noted that only a small fraction of carriers of *ABCA4* mutations develop this particular phenotype (1/60). The latter finding may be indicative of a role for other unknown modifiers that contribute to this specific phenotype in the presence of a heterozygous mutant *ABCA4* allele.

Heterozygous mutations in *ABCA4* (p.V2050L) have also been reported to contribute to an exacerbation of the phenotype conferred by a monoallelic mutation in *PRPH2* (p.R172W).[41] In another study, 12 nonsymptomatic mutation-carrying relatives of STGD1 patients were found to have normal visual acuity but impaired contrast sensitivity and reduced multifocal ERG amplitudes.[21] More recently, a subset of *ABCA4* carriers were reported to have reduced visual acuity, fundus abnormalities that included pigmentary changes (8/18) and flecks, and multifocal ERGs of reduced amplitude and delayed implicit times.[22] Some missense mutations, including the complex allele p.[L541P;A1038V], have been shown to be associated with ABCA4 mislocalization; the p.L541P mutation in particular prevents correct localization of ABCA4 in OS and thus retention in inner segments.[42] It is expected that under these conditions the pathogenesis of STGD1 could be exacerbated by endoplasmic reticulum (ER) stress and the unfolded-protein response (UPR).[43] Since the onset of the UPR may be dependent on mutation type and gene dosage, a monoallelic p.[L541P; A1038V] mutation may leave photoreceptor cells with a limited and latent capacity to deal with other sources of ER stress.

Only four carriers had fundus abnormalities in the form of central fleck-like changes. The foci of increased and decreased AF signals corresponded to hyper- and hyporeflective deposits traversing the photoreceptor-attributable bands in the SD-OCT images. The pathognomonic significance of this observation remains to be elucidated. In addition, quantitative analysis of the SD-OCT images showed that for the majority of carriers there was no clear trend toward thinning or thickening of the segmented retinal layers.

Limitations of our study included age restrictions. For instance, subjects older than age 60 were not included in the qAF analysis because of reduced ocular media transmission. Nevertheless, these older subjects may reveal changes that are not detectable at earlier ages. Imaging of pseudophakic subjects could enable the study of these older age groups. Perhaps if we had used psychophysical and electrophysiological tests,[21] other changes would have been revealed. All abnormal fleck-like changes we observed (S7.2, S9.3, S41.2, S43.2) were situated perifoveally, while qAF_8 measurements were taken at an eccentricity of 7° to 9° (see Fig. 1), a location outside the area of fundus change. Another limitation of this study is that the control group was not genotyped for *ABCA4*. Given the estimated carrier frequency of ~5% in the general population, we cannot exclude that some of the healthy control subjects were actually carrying a disease-associated *ABCA4* allele.

In summary, we observed somewhat unexpectedly that most individuals between the ages of 9 and 60 who are heterozygous for disease-causing mutations in *ABCA4* do not present with qAF levels higher than the normal range. In four carriers, central fleck-like changes were visible in SW-AF and SD-OCT images. Otherwise, carriers had normal retinal structure on SD-OCT.

Acknowledgments

Supported in part by grants from the National Eye Institute/National Institutes of Health EY024091, EY021163, EY019007; Arnold and Mabel Beckman Foundation; Foundation Fighting Blindness; a grant from Research to Prevent Blindness to the Department of Ophthalmology, Columbia University; Robert L. Burch III Fund, Columbia University, New York, New York, United States; New York Community Trust–Fredrick J. and Theresa Dow Wallace Fund, Columbia University, New York, New York, United States. The authors alone are responsible for the content and writing of the paper.

Disclosure: **T. Duncker**, None; **G.E. Stein**, None; **W. Lee**, None; **S.H. Tsang**, None; **J. Zernant**, None; **S. Bearelly**, None; **D.C. Hood**, None; **V.C. Greenstein**, None; **F.C. Delori**, None; **R. Allikmets**, None; **J.R. Sparrow**, None

References

1. Molday LL, Rabin AR, Molday RS. ABCR expression in foveal cone photoreceptors and its role in Stargardt macular dystrophy. *Nat Genet*. 2000;25:257–258.
2. Sun H, Nathans J. Stargardt's ABCR is localized to the disc membrane of retinal rod outer segments. *Nat Genet*. 1997;17:15–16.
3. Papermaster DS, Schneider BG, Zorn MA, Kraehenbuhl JP. Immunocytochemical localization of a large intrinsic membrane protein to the incisures and margins of frog rod outer segment disks. *J Cell Biol*. 1978;78:415–425.
4. Weng J, Mata NL, Azarian SM, Tzekov RT, Birch DG, Travis GH. Insights into the function of Rim protein in photoreceptors and etiology of Stargardt's disease from the phenotype in abcr knockout mice. *Cell*. 1999;98:13–23.
5. Kim SR, Jang YP, Jockusch S, Fishkin NE, Turro NJ, Sparrow JR. The all-trans-retinal dimer series of lipofuscin pigments in retinal pigment epithelial cells in a recessive Stargardt disease model. *Proc Natl Acad Sci U S A*. 2007;104:19273–19278.
6. Yamamoto K, Yoon KD, Ueda K, Hashimoto M, Sparrow JR. A novel bisretinoid of retina is an adduct on glycerophosphoethanolamine. *Invest Ophthalmol Vis Sci*. 2011;52:9084–9090.
7. Sparrow JR, Gregory-Roberts E, Yamamoto K, et al. The bisretinoids of retinal pigment epithelium. *Prog Retin Eye Res*. 2012;31:121–135.
8. Wu L, Nagasaki T, Sparrow JR. Photoreceptor cell degeneration in *Abcr*$^{-/-}$ mice. *Adv Exp Med Biol*. 2010;664:533–539.
9. Eagle RC Jr, Lucier AC, Bernardino VB Jr, Yanoff M. Retinal pigment epithelial abnormalities in fundus flavimaculatus: a light and electron microscopic study. *Ophthalmology*. 1980;87:1189–1200.
10. Cideciyan AV, Aleman TS, Swider M, et al. Mutations in ABCA4 result in accumulation of lipofuscin before slowing of the retinoid cycle: a reappraisal of the human disease sequence. *Hum Mol Genet*. 2004;13:525–534.
11. Allikmets R, Singh N, Sun H, et al. A photoreceptor cell-specific ATP-binding transporter gene (ABCR) is mutated in recessive Stargardt macular dystrophy. *Nat Genet*. 1997;15:236–246.
12. Martinez-Mir A, Paloma E, Allikmets R, et al. Retinitis pigmentosa caused by a homozygous mutation in the Stargardt disease gene ABCR. *Nat Genet*. 1998;18:11–12.
13. Cremers FP, van de Pol DJ, van Driel M, et al. Autosomal recessive retinitis pigmentosa and cone-rod dystrophy caused by splice site mutations in the Stargardt's disease gene ABCR. *Hum Mol Genet*. 1998;7:355–362.

14. van Driel MA, Maugeri A, Klevering BJ, Hoyng CB, Cremers FP. ABCR unites what ophthalmologists divide(s). *Ophthalmic Genet*. 1998;19:117–122.
15. Jaakson K, Zernant J, Kulm M, et al. Genotyping microarray (gene chip) for the ABCR (ABCA4) gene. *Hum Mutat*. 2003; 22:395–403.
16. Yatsenko AN, Shroyer NF, Lewis RA, Lupski JR. Late-onset Stargardt disease is associated with missense mutations that map outside known functional regions of ABCR (ABCA4). *Hum Genet*. 2001;108:346–355.
17. Fritsche LG, Fleckenstein M, Fiebig BS, et al. A subgroup of age-related macular degeneration is associated with monoallelic sequence variants in the ABCA4 gene. *Invest Ophthalmol Vis Sci*. 2012;53:2112–2118.
18. Allikmets R, Shroyer NF, Singh N, et al. Mutation of the Stargardt disease gene (ABCR) in age-related macular degeneration. *Science*. 1997;277:1805–1807.
19. Souied EH, Ducroq D, Gerber S, et al. Age-related macular degeneration in grandparents of patients with Stargardt disease: genetic study. *Am J Ophthalmol*. 1999;128:173–178.
20. Zhang R, Wang LY, Wang YF, et al. Associations of the G1961E and D2177N variants in ABCA4 and the risk of age-related macular degeneration. *Gene*. 2015;567:51–57.
21. Maia-Lopes S, Silva ED, Silva MF, Reis A, Faria P, Castelo-Branco M. Evidence of widespread retinal dysfunction in patients with stargardt disease and morphologically unaffected carrier relatives. *Invest Ophthalmol Vis Sci*. 2008;49:1191–1199.
22. Kjellstrom U. Reduced macular function in ABCA4 carriers. *Mol Vis*. 2015;21:767–782.
23. Delori FC, Staurenghi G, Arend O, Dorey CK, Goger DG, Weiter JJ. In vivo measurement of lipofuscin in Stargardt's disease–Fundus flavimaculatus. *Invest Ophthalmol Vis Sci*. 1995;36:2327–2331.
24. Burke TR, Duncker T, Woods RL, et al. Quantitative fundus autofluorescence in recessive Stargardt disease. *Invest Ophthalmol Vis Sci*. 2014;55:2841–2852.
25. Mata NL, Tzekov RT, Liu X, Weng J, Birch DG, Travis GH. Delayed dark-adaptation and lipofuscin accumulation in abcr+/- mice: implications for involvement of ABCR in age-related macular degeneration. *Invest Ophthalmol Vis Sci*. 2001;42:1685–1690.
26. Sparrow JR, Blonska A, Flynn E, et al. Quantitative fundus autofluorescence in mice: correlation with HPLC quantitation of RPE lipofuscin and measurement of retina outer nuclear layer thickness. *Invest Ophthalmol Vis Sci*. 2013;54:2812–2820.
27. Delori F, Greenberg JP, Woods RL, et al. Quantitative measurements of autofluorescence with the scanning laser ophthalmoscope. *Invest Ophthalmol Vis Sci*. 2011;52:9379–9390.
28. Greenberg JP, Duncker T, Woods RL, Smith RT, Sparrow JR, Delori FC. Quantitative fundus autofluorescence in healthy eyes. *Invest Ophthalmol Vis Sci*. 2013;54:5684–5693.
29. van de Kraats J, van Norren D. Optical density of the aging human ocular media in the visible and the UV. *J Opt Soc Am A Opt Image Sci Vis*. 2007;24:1842–1857.
30. Yang Q, Reisman CA, Chan K, Ramachandran R, Raza A, Hood DC. Automated segmentation of outer retinal layers in macular OCT images of patients with retinitis pigmentosa. *Biomed Opt Express*. 2011;2:2493–2503.
31. Hood DC, Cho J, Raza AS, Dale EA, Wang M. Reliability of a computer-aided manual procedure for segmenting optical coherence tomography scans. *Optom Vis Sci*. 2011;88:113–123.
32. Bland JM, Altman DG. Statistical methods for assessing agreement between two methods of clinical measurement. *Lancet*. 1986;1:307–310.
33. Bottoni F, Fatigati G, Carlevaro G, De Molfetta V. Fundus flavimaculatus and subretinal neovascularization. *Graefes Arch Clin Exp Ophthalmol*. 1992;230:498–500.
34. von Aulock S, Schroder NW, Traub S, et al. Heterozygous toll-like receptor 2 polymorphism does not affect lipoteichoic acid-induced chemokine and inflammatory responses. *Infect Immun*. 2004;72:1828–1831.
35. Charbel Issa P, Barnard AR, Singh MS, et al. Fundus autofluorescence in the Abca4(-/-) mouse model of Stargardt disease–correlation with accumulation of A2E, retinal function, and histology. *Invest Ophthalmol Vis Sci*. 2013;54:5602–5612.
36. Allikmets R. Further evidence for an association of ABCR alleles with age-related macular degeneration. The international ABCR Screening Consortium. *Am J Hum Genet*. 2000; 67:487–491.
37. Fishman GA, Stone EM, Grover S, Derlacki DJ, Haines HL, Hockey RR. Variation of clinical expression in patients with Stargardt dystrophy and sequence variations in the ABCR gene. *Arch Ophthalmol*. 1999;117:504–510.
38. De La Paz MA, Guy VK, Abou-Donia S, et al. Analysis of the Stargardt disease gene (ABCR) in age-related macular degeneration. *Ophthalmology*. 1999;106:1531–1536.
39. Stone EM, Webster AR, Vandenburgh K, et al. Allelic variation in ABCR associated with Stargardt disease but not age-related macular degeneration. *Nat Genet*. 1998;20:328–329.
40. Shroyer NF, Lewis RA, Yatsenko AN, Wensel TG, Lupski JR. Cosegregation and functional analysis of mutant ABCR (ABCA4) alleles in families that manifest both Stargardt disease and age-related macular degeneration. *Hum Mol Genet*. 2001; 10:2671–2678.
41. Poloschek CM, Bach M, Lagreze WA, et al. ABCA4 and ROM1: implications for modification of the PRPH2-associated macular dystrophy phenotype. *Invest Ophthalmol Vis Sci*. 2010;51: 4253–4265.
42. Wiszniewski W, Zaremba CM, Yatsenko AN, et al. ABCA4 mutations causing mislocalization are found frequently in patients with severe retinal dystrophies. *Hum Mol Genet*. 2005;14:2769–2778.
43. Cideciyan AV, Swider M, Aleman TS, et al. ABCA4 disease progression and a proposed strategy for gene therapy. *Hum Mol Genet*. 2009;18:931–941.
44. Staurenghi G, Sadda S, Chakravarthy U, Spaide RF. Proposed lexicon for anatomic landmarks in normal posterior segment spectral-domain optical coherence tomography. *Ophthalmology*. 2014;121:1572–1578.
45. Duncker T, Tsang SH, Lee W, et al. Quantitative fundus autofluorescence distinguishes ABCA4-associated and non-ABCA4-associated bull's-eye maculopathy. *Ophthalmology*. 2015;122:345–355.
46. Duncker T, Tsang SH, Woods RL, et al. Quantitative fundus autofluorescence and optical coherence tomography in PRPH2/RDS- and ABCA4-associated disease exhibiting phenotypic overlap. *Invest Ophthalmol Vis Sci*. 2015;56:3159–3170.

Investigative Ophthalmology & Visual Science